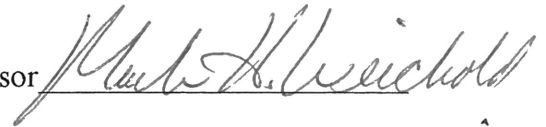


Effects of Lateral Confinement in a Superlattice

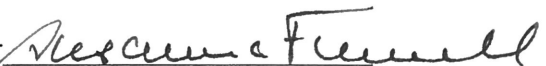
Julio Toro Silva  
University Undergraduate Fellow, 1995-1996  
Texas A&M University  
Department of Electrical Engineering

APPROVED

Fellows Advisor



Honors Director



## EFFECTS OF LATERAL CONFINEMENT IN A SUPERLATTICE

### Abstract

We discuss the progress that we have had in studying the effects that lateral confinement has in the electronic bandstructure of a superlattice, and consequently, on its current-voltage characteristics. This study has been divided into several parts. First, we study devices that make use peculiarities in their electronic bandstructure in order to understand the possible applications of a custom-made bandstructure. Then, we concentrate on superlattices and their properties. Next, we will try to put forward a hypothesis of the effect that the lateral confinement of electrons in a superlattice will have in the electronic bandstructure of the superlattice. Finally, we will mention the methods that we are using to try to verify our hypothesis on lateral confinement of superlattices.

Although we do not have any specific results that would verify the hypothesis that lateral confinement of a superlattice affects its electronic bandstructure and I-V characteristics, we present a summary of other experiments that try to confine carriers laterally in semiconductors using different fabrication techniques. We believe that these experiments will help us have a better idea of the effects of lateral confinement. Our work in simulating the electronic bandstructure of a superlattice when it is laterally confined is still going on.

# EFFECTS OF LATERAL CONFINEMENT IN A SUPERLATTICE

## Table of Contents

	ABSTRACT	ii
	INTRODUCTION	iv
1	TRANSFERRED ELECTRON DEVICES	1
	1.1 Gunn Diodes	1
	1.2 The Gunn Effect	1
	1.3 Properties of a good Gunn diode	5
	1.4 Indium Phosphide Gunn diodes	7
	1.5 Comparison between different semiconductor materials	9
2	SUPERLATTICES	11
	2.1 Structure of a superlattice	11
	2.2 Classification of a superlattice	12
	2.3 Fabrication	13
	2.4 Bandstructure of superlattices	15
	2.5 Practical example: negative differential conductance in superlattices	19
3	TWO DIMENSIONAL CONFINEMENT IN SEMICONDUCTORS	21
	3.1 Theory	21
	3.2 Fabrication of 1-D semiconductor structures	22
	3.3 Two dimensional confinement in superlattices	25
	3.4 The tight binding method	27
	REFERENCES	32
	APPENDIX A - Matlab program	35
	APPENDIX B - Mathcad program	39

## **EFFECTS OF LATERAL CONFINEMENT IN A SUPERLATTICE**

### **Introduction**

Bandgap engineering, the manipulation of individual layers of atoms in crystal grown on a wafer to achieve useful properties that would otherwise not exist, has become something of a Holy Grail for solid state physicists and engineers. However, bandgap engineering is still in its infancy. What has made it possible are new fabrication techniques. These new techniques of semiconductor crystal growth have given engineers and physicists extremely precise control of layer thickness. For instance, with molecular beam epitaxy (MBE), it is possible to grow just one layer of atoms at a time on a semiconductor wafer. Although very expensive, this approach obviously guarantees a virtually perfect crystal structure. When we start building devices that have layers of one or a few atoms, the physics of the device must change as we enter the quantum realm.

Semiconductor devices consisting of hundreds of such superthin layers behave very differently from those made of bulk crystal. Engineers can tailor-make devices to yield a whole range of otherwise unobtainable but useful electronic or optical properties. What is being changed is the electronic bandstructure of the material. For example, a GaAs-AlAs superlattice will not have the same bandstructure as a GaAlAs alloy. The bandgap of the semiconductor material, or the difference in energy between the conduction and the valence band, is being changed. Also, new "bandgaps" are being created. There will be several extra energy levels in both the conduction and valence bands.

The electronic bandstructure of a semiconductor defines many of its properties. Through bandgap engineering, we can raise or lower the velocity at which electrons or holes may

The electronic bandstructure of a semiconductor defines many of its properties. Through bandgap engineering, we can raise or lower the velocity at which electrons or holes may travel through a lattice of atoms. We can also raise or lower the bandgap of the semiconductor. If it is a direct gap semiconductor, we would be able to tune the wavelength of the light emitted by raising and lowering the bandgap.

There are essentially three tools that are used by bandgap engineers: alloying, which changes the chemical composition of a semiconductor; the introduction of mechanical strain between crystal layers; and the juxtaposition of heterogeneous materials to form heterojunctions. We will concentrate on the last method.

In superlattices, an artificial bandstructure is created. In studying the effects of lateral confinement of carriers in the electronic bandstructure of a superlattice, we hope to provide a means to adjust the electronic structure of the superlattice after its fabrication has been completed.

## **EFFECTS OF LATERAL CONFINEMENT IN A SUPERLATTICE**

### **I. Transferred Electron Devices**

In order to understand how practical and useful it is to have a variety of electronic bandstructures, we first studied devices that use peculiarities in their bandstructure as an advantage. There are several examples of these devices, but we chose to use the transferred electron devices, also known as Gunn diodes or Gunn oscillators, because they have some characteristics that we believe can be improved in a superlattice.

#### **1.1 Gunn Diodes**

The Gunn diode is a transferred electron two-terminal device with very important practical applications at microwave frequencies. These devices are widely used as radar local oscillators and as transmitters for low-power radars. Gunn diodes have much larger efficiencies than those obtained with the best power transistors at RF frequencies. They are used for microwave generation and amplification. Their operating frequency range is from 5 to 25 GHz and their continuous power is up to a few hundred milliwatts.

#### **1.2 The Gunn Effect**

The transferred electron effect, or Gunn effect, was first discovered by J.B. Gunn in 1963. He was testing a number of thin specimens made of n-type GaAs and n-type InP. Gunn found out that above some critical voltage, the current in every specimen became a fluctuating function of time. In the GaAs specimens, this fluctuation took the form of a periodic oscillation superimposed upon the pulse current .[1]

Gunn established that the period of oscillation was usually inversely proportional to the length of the specimen and closely equal to the transit time of electrons between the electrodes. The theoretical basis for explaining the Gunn effect already existed in papers by Ridley and Watkins [2] and Hilsum [3]; however, Gunn dismissed them as unrelated. The Gunn effect can be explained if it is assumed that these semiconductors have a negative differential bulk conductivity above the oscillation threshold and that the current oscillations are due to the periodic nucleation and disappearance of traveling space-charge instability domains. This negative mobility is a result of the conduction band structure of GaAs and other semiconductors. Figure 1.1 shows the current-voltage characteristics of a semiconductor with a negative resistance region.  $V_{th}$  represents the threshold voltage at which the negative differential conductance and the oscillations start.

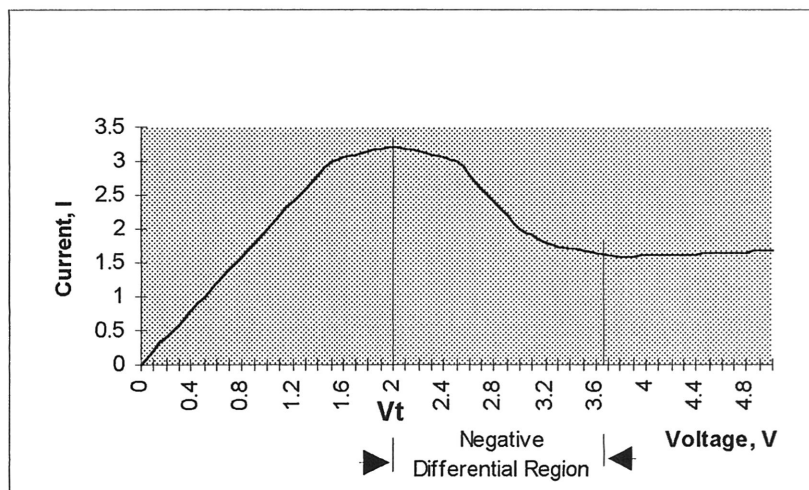


**Figure 1.1** I-V characteristics.

GaAs is a direct gap semiconductor with a conduction band minimum occurring at  $k=0$ , the center of the Brillouin zone. It is typical of direct gap semiconductors that the

conduction band effective mass is relatively low, and GaAs is no exception to this rule. In addition to this central valley, GaAs possesses satellite valleys; that is, additional conduction band minima with higher effective masses at higher energies. These energies are large compared to  $kT$ . In the particular case of GaAs, the minimum of the satellite valley is at about 0.36 eV from the minimum of the central valley. Figure 1.2 shows a simplified bandstructure of Gallium Arsenide.

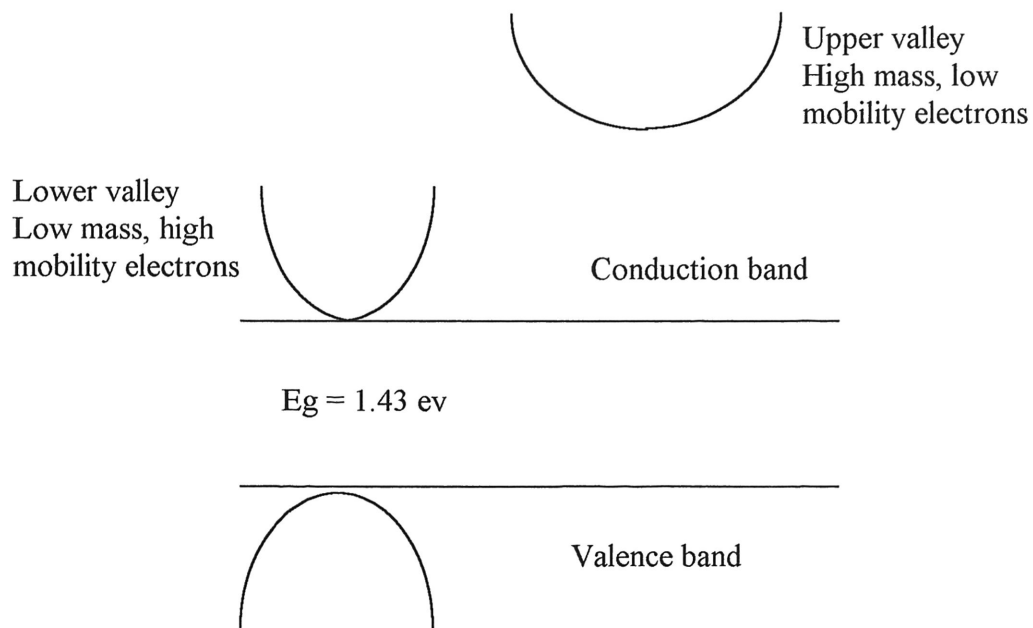


**Figure 1.2** Simplified bandstructure of GaAs.

At room temperature, and in the absence of any electric fields, all electrons will occupy the central valley since the energy separation between it and the satellite valleys is large compared to  $kT$ . Because of the very low effective mass in the central valley, the electrons have the high mobility that is characteristic of these semiconductors; but, for the same reason, the electrons are also very easily heated by an external electric field. When



this heating takes place, an increasing fraction of electrons reaches energies approaching the magnitude of the satellite-valley energies, thereby becoming scattered into these valleys. The large effective mass of the satellite valleys and the possibility of intervalley scattering between them cause the mobility of these high-energy electrons to be much lower than the mobility of the central valley electrons. As a result, the overall average electron mobility and conductivity of such a crystal will decrease as soon as the electric field reaches a value large enough to sustain electron transfer into the satellite valleys. Once the electron transfer has started, the fraction of high-energy electrons steeply increases with the increasing electric field. Even though the velocity of those electrons that stay behind in the central valley keeps increasing in proportion to the electric field, the rate of electron loss from the high velocity central valley into the low velocity satellite valleys is so rapid that, above a certain threshold field, the current, and therefore, the average drift velocity, actually drops with further increase of the electric field, leading to the negative differential mobility that is observed. [4] In GaAs, this threshold field is somewhere between 3.0 and 3.5 kV/cm, and the transfer appears to be complete at about 20 kV/cm.

Similar behavior can be expected for any other semiconductor with a similar bandstructure: a low-mass central valley and a set of high-mass satellite valleys. There are several semiconductors that fulfill these requirements and exhibit the Gunn effect: InP, InAs, GaAs, CdTe, and ZnSe among others.

### 1.3 Properties of a good Gunn Diode

Usually, engineers have to deal with the characteristics of a material as given. However, our purpose is to determine what are the characteristics that make a good Gunn device in order to try to emulate these characteristics.

- a. The separation of energy between the bottom of the lower valley and the bottom of the upper valley must be several times larger than the thermal energy ( $kT$ ) at room temperature to ensure that no significant interaction between the bands occurs before the field is great enough to heat the upper band electrons. This reduces the possibility of impact ionization, which we do not want, and reduces the noise. The condition for separation is  $E \geq 13kT$ .
- b. The separation between the valleys must be smaller than the gap energy between the conduction and valence bands. Otherwise, the semiconductor will break down and become highly conductive before the electrons begin to transfer to the upper valleys because large amounts of electron-hole pairs are created.
- c. Electrons in the lower valley must have high mobility (small effective mass) and a low density of states whereas those in the upper valley must have low mobility (high effective mass) and a high density of states.

d. The transfer process must be efficient so that the number of electrons in the satellite valley becomes appreciably larger than the number of electrons in the central valley within a small range of the applied electric field to ensure a negative differential mobility.

e. The transfer of energy to the lattice must be through optical polar mode scattering. This creates a strong field dependence of electron temperature, yet the mobility will not vary strongly with field. The scattering of electrons through the acoustical mode must be very low.

f. A rise of lattice temperature with increasing field is inevitable, and luckily, it is also advantageous.

g. Short intervalley scattering times. This creates a more pronounced negative differential conductance.

h. Impurity scattering must be negligible so that the density of ionized impurities be kept low. This property depends on the cleanliness of our fabrication process.

i. For most application purposes, we want a large peak drift velocity of the electrons, which translates into a large peak current.

j. Also for most applications, we want a relatively small threshold voltage. In addition, at lower electric fields, there is less noise.

k. High resistivity material.

l. We want to avoid injection from the contacts of the diode. It increases the density as the field is increased and therefore jeopardizes the achievement of negative resistance.

Ohmic contacts are desirable.

To determine how good is a Gunn device, we can study its current-voltage characteristics. First, we want a large peak current and a low threshold voltage. Most important of all, we want a large ratio of peak current flow to valley current flow. This ratio is related to the band structure and scattering mechanisms of the device, and it determines the efficiency of the Gunn oscillator/amplifier.

#### **1.4 Indium Phosphide Gunn Diodes**

Besides having an upper-valley energy level and a lower-valley energy level like GaAs, indium phosphide (InP) also has a third middle-valley energy level. The energy difference between the upper and lower valleys is about 0.8 eV, whereas the energy difference between the middle and lower valleys is close to 0.6 eV.

In GaAs, the electron transfer process from the lower valley to the upper valley is comparatively slow. At a particular voltage above threshold, current flow consists of a larger contribution of electrons from the lower valley rather than from the upper valley. Because of this larger contribution from the lower energy level, a relatively low peak-to-valley current ratio results.

The InP diode has a larger peak-to-valley current ratio because electron transfer proceeds rapidly as the field increases. This transfer occurs because the coupling between the lower valley and upper valley in InP is weaker than in GaAs. The middle-valley energy level provides the additional energy loss mechanism required to avoid breakdown due to the high energies acquired by the lower-valley electrons from the weak coupling. Under normal operating conditions, electrons concentrate in the middle valley. Because InP has a greater energy separation between the lower valley and the nearest energy levels, the thermal excitation of electrons has less effect and the degradation of its peak-to-valley current ratio is about four times less than in GaAs. [5] Kamoua *et al* present a good review of the literature on the material parameters of InP, including energy separation, effective mass, intervalley coupling constant, acoustic deformation potential, LO phonon energy, static dielectric constant, and optical dielectric constant. [6]

### 1.5 Comparison between different semiconductor materials

The two most important materials that show the Gunn effect are GaAs and InP. InP has a high peak-to-valley current ratio, while GaAs has a lower threshold voltage. Other materials in which the Gunn effect has been observed are InAs, GaInAs, GaAsP, and CdTe.

The intrinsic 3 dB cutoff frequency of the negative differential mobility is of about 40 GHz for GaInAs, 100 GHz for GaAs, and 200 GHz for InP. The best experimental results published so far for these conventional devices are 150 mW output power with 3.6% efficiency for InP at 94 GHz and 96 mW with 2.7% efficiency at 94 GHz also for GaAs.[7]

For CdTe samples, the response to pulsed electric fields is quite similar to that of GaAs, except for a higher threshold field. A major difference with GaAs is the substantially higher threshold field, about 13 kV/cm as compared with about 3 kV/cm for GaAs. Similar maximum efficiencies are expected for CdTe and GaAs, and it is also expected that they operate at about the same frequency. The higher threshold field of CdTe coupled with its comparatively poor thermal conductivity makes it unlikely that microwave Gunn devices can be fabricated from it. [8]

Alloys of InAs and GaAs can be expected to yield a higher mobility than GaAs and a wider energy gap than InAs. Furthermore, the difference between the central and satellite valleys in the conduction band becomes wider with the increase of the composition rate of InAs. This tends to make a maximum velocity higher than that of GaAs. Also, the InGaAs alloy has a smaller threshold field than GaAs and a substantially larger mobility

and peak velocity. InGaAs alloys yield a very interesting conversion efficiency below 40 GHz, but have a reduced cutoff frequency as compared to GaAs and InP. [9] [10]

GaAs and GaP form a continuous series of solid solutions, and as one goes from GaAs to  $\text{GaAs}_{0.5}\text{P}_{0.5}$  the separation between the  $\langle 000 \rangle$  and  $\langle 100 \rangle$  minima decreases from about 0.36 eV to zero. The threshold field therefore decreases as one goes across the series, and for phosphorus concentrations greater than 0.5, the oscillations do not longer occur. The main advantage of this alloy is the lower threshold field. [11]

## EFFECTS OF LATERAL CONFINEMENT IN A SUPERLATTICE

### II. Superlattices

We mentioned that one of the methods that bandgap engineers use is the juxtaposition of heterogeneous materials to form heterojunctions. With two of these heterojunctions we can create a quantum well. Now consider a periodic structure with many quantum wells. The barrier layers should be thin enough to allow significant tunneling. The perpendicular kinetic energy of electrons in such a structure breaks up into allowed bands separated by forbidden gaps, just as we would expect in any periodic structure. Of course, this is analogous to the formation of energy bands in solids in consequence of their periodic crystal lattices.

#### 2.1 Structure of a superlattice

The term superlattice generally refers to structures where the barrier layer is thin, so there is appreciable interaction between the wave functions in neighboring wells. Research in semiconductor superlattices was initiated in 1969 in a paper by Esaki and Tsu. [12]

Although the original proposal was to achieve a negative differential conductivity in semiconductors, the subject of superlattices has since generated a great deal of activities to gain a better understanding of these artificial semiconductor structures as well to invent new devices to meet engineering needs.

There are important differences between the natural crystal lattice and the artificial superlattice. First, the period of the superlattice is typically between 30 and 100



Angstroms ( $\text{\AA}$ ), whereas the period of the crystal lattice is only a few Angstroms.

Therefore, the energy bands of the superlattice, which arise from the coupling between the energy levels of the potential wells, are typically much narrower (on the order of 10 meV) than those on the crystal; they are called minibands. Second, the superlattice is generally one-dimensional, unlike the three-dimensional crystal lattice. [13]

The creation of the minibands in a superlattice would allow for the observation of familiar quantum mechanical properties in a new domain of physical scale. Esaki and Tsu [12] were the first to notice that in the direction of the superlattice (perpendicular to the superlattice planes), the narrow wave-vector zones and the narrow energy bands make it possible for electrons to be excited beyond the energy corresponding to an  $E$  vs.  $k$  inflection point with moderate electric fields. This would result in negative conductance that could lead to new ultra high-speed devices. These devices would have virtually no frequency limitation, except when the energy quantum for the frequency involved is a significant fraction of the width of the narrow energy band.

## 2.2 Classification of Superlattices

Superlattices that have been grown can be placed in three general categories: lattice matched, strained, and strained with intermediate substrate. [14] In the lattice matched superlattices, such as GaAs/AlAs and HgTe/CdTe, there is a very good match between the lattice constants of the two components forming the superlattice. These superlattices are the easiest to grow; the highest quality superlattices fall in this category.

The strained superlattices are those where the components have different lattice constants, and one of the components is considered the substrate. The thickness of the coherent superlattice is limited by the competition between the strain energy in the non-substrate component and the dislocation formation energy. The strained superlattice can be grown only up to a limited thickness before dislocations are generated. When the dislocations are generated, there is no longer a one-to-one correspondence between the atoms across various planes of the structure. This leads to undesirable changes in the electrical and optical properties.

To avoid the problems caused by dislocations and still utilize the benefits of built-in strain, a substrate with an intermediate lattice constant can be used. However, often the substrates that are available are limited.

### **2.3 Fabrication**

Heteroepitaxy is fundamental for the growth of a superlattice. Steady improvements in grow techniques such as molecular beam epitaxy (MBE) and metalorganic chemical vapor deposition (MOCVD) during the last decade have made possible high-quality heterostructures having designed potential profiles and impurity distributions with dimensional control close to interatomic spacing and with virtually defect-free interfaces, particularly in lattice-matched superlattices. In addition to MBE and MOCVD, new or unconventional techniques such as GS (gas source) MBE [15], LP (low pressure) MOCVD [16], CBE (chemical beam epitaxy) [17], HWE (hot wall epitaxy) [18], and ALE (atomic layer epitaxy) [19] have been explored.

MBE, MOCVD, and the other techniques allow monolayer (about 3 Angstroms) control in the chemical composition of the growing crystal. The basic components of a typical MBE growth system are banks of Knudson cells containing the charges for the various elements to be deposited. Materials for the host crystal as well as the dopants are contained here. Highly reliable fast shutters are mounted in front of the cells to allow abrupt change in chemical composition of the crystal. The crystal grows at a rate of about one monolayer per second or about a micron per hour. The substrate on which the growth occurs is heated to an appropriate level. For optimum control and calibration, *in situ* monitoring techniques, such as Reflection High Energy Electron Diffraction (RHEED), are mounted on the system. [14]

Nearly every semiconductor extending from zero bandgap (HgCdTe) to large bandgap materials such as ZnSe, CdS, etc., has been grown by epitaxial techniques such as MBE and MOCVD. In MBE, atoms or molecules of the species to be grown impinge upon the substrate in high vacuum. In MOCVD, the impinging species are complex molecules containing the atoms which are to form the crystal, and a dissociative chemisorption reaction occurs at the surface.

Since the new heteroepitaxial techniques allow one to grow heterostructures with atomic control, one can change the periodicity of the crystal in the growth direction.

## 2.4 Bandstructure of Superlattices

The increase in the real space periodicity distance has very important consequences for the bandstructure of a superlattice. In the plane of growth, the periodicity distance is still given by the face-centered cubic (fcc) unit cell. However, in the growth direction, the periodicity has increased to several times the previous value. This means that  $k$ -space periodicity or the reciprocal lattice vector in the  $x$ -direction has decreased by the same factor. The extent of the first Brillouin zone has therefore decreased.

The imposition of the background periodic potential causes the formation of new bandgaps and also alters the effective mass of the composite material.

A simple way to address the superlattice problem is to use the effective mass theory via the Kronig-Penney model. This model is very useful to introduce the concepts of minibands and zone folding. In the Kronig-Penney model, we assume that the electron is described by an effective mass corresponding to the conduction band or valence band of the semiconductor forming the superlattice, and it simply sees a superimposed periodic potential.

The general Schrödinger equation is of the form

$$[-(\hbar^2/8\pi^2m) (\partial^2/\delta x^2) + V(x)] \psi(x) = E\psi(x) \quad (2.1)$$

where  $V(x)$  is the background potential. The effective mass  $m$  for the material at  $x$  can be different for different regions. Note that we have suppressed the Schrödinger equation in the plane perpendicular to the superlattice potential. The energy due to the momentum in this perpendicular plane is given by

$$E_{\parallel}(k_{\parallel}) = \hbar^2 k_{\parallel}^2 / 8\pi^2 m \quad (2.2)$$

This perpendicular energy must be added to the results obtained by the solution of equation 2.1. Due to the periodic nature of the potential  $V(x)$ , the solution of Equation 2.1 must satisfy the Bloch theorem, i.e.

$$\psi(x+d) = e^{i\phi} \psi(x) \quad (2.3)$$

where  $\phi = k_x d$  and the period  $d$  is  $d = a + b$ .

In the period  $-b < x < a$ , let

$$\psi(x) = A e^{i\beta x} + B e^{-i\beta x}, \text{ if } -b < x < 0 \quad (2.4)$$

$$\psi(x) = D e^{i\alpha x} + F e^{-i\alpha x}, \text{ if } 0 < x < a$$

where

$$\beta = [8\pi^2 m(E - V_0)/\hbar^2]^{1/2}$$

$$\alpha = [8\pi^2 mE/\hbar^2]^{1/2}$$

Then, in the following period,  $a < x < a + d$ ,

$$\psi(x) = e^{i\phi} [A e^{i\beta(x-d)} + B e^{-i\beta(x-d)}], \text{ if } a < x < d \quad (2.5)$$

$$\psi(x) = e^{i\phi} [D e^{i\alpha(x-d)} + F e^{-i\alpha(x-d)}], \text{ if } d < x < a + d$$

From the continuity conditions at  $x = 0$  and at  $x = a$ , the following system of equations is obtained

$$A + B = D + F \quad (2.6)$$

$$\beta(A - B) = \alpha(D - F)$$

$$e^{i\phi} [A e^{i\beta b} + B e^{-i\beta b}] = e^{i\phi} [D e^{i\alpha a} + F e^{-i\alpha a}]$$

$$\beta e^{i\phi} [A e^{i\beta b} - B e^{-i\beta b}] = \alpha e^{i\phi} [D e^{i\alpha a} - F e^{-i\alpha a}]$$

Non-trivial solutions for the variables  $A$ ,  $B$ ,  $D$ , and  $F$  are obtained only if the determinant of their coefficient vanishes, which gives the condition

$$\cos \phi = \cos a\alpha \cosh b\delta - (\alpha^2 - \delta^2)/2\alpha\delta \sin a\alpha \sinh b\delta, \text{ if } 0 < E < V_0 \quad (2.7)$$

$$\cos \phi = \cos a\alpha \cos b\beta - (\alpha^2 + \beta^2)/2\alpha\delta \sin a\alpha \sin b\beta, \text{ if } E > V_0$$

where

$$\delta = [8\pi^2 m(V_0 - E)/h^2]^{1/2}$$

Now the energy  $E$  is physically allowed only if

$$-1 \leq \cos \phi \leq +1 \quad (2.8)$$

We distinguish two cases:

1.  $0 < E < V_0$ . To get a picture of the structure of the energy spectrum, we look at the particular case for which  $b \rightarrow 0$ ,  $\delta \rightarrow \infty$ , in such a manner that  $b\delta^2$  remains finite. With the notation

$$P = \lim (a b \delta^2)/2 \text{ as } b \rightarrow 0, \delta \rightarrow \infty$$

equation 2.8 becomes

$$-1 \leq P (\sin a\alpha)/a\alpha + \cos a\alpha \leq +1 \quad (2.9)$$

By plotting this equation, it can be seen that the energy spectrum consists of a series of separate regions, inside each of which, the energy of the particle can vary continuously. These regions are the "allowed bands," or minibands, and the ones between them are the "forbidden bands." It can be seen that the width of the allowed bands increases as the energy increases. Figure 2.1 shows a plot of equation 2.9.

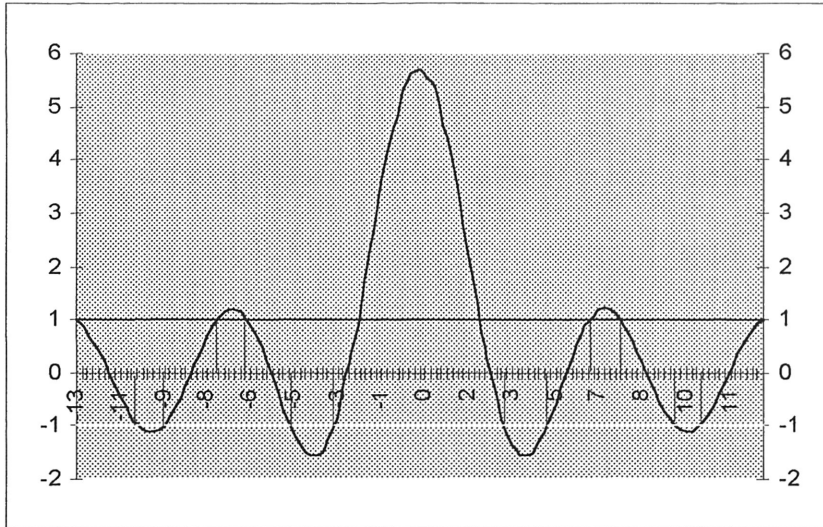


**Figure 2.1** Positions of allowed bands.  
 $a\alpha$  on the x axis.  $P(\sin a\alpha)/a\alpha + \cos a\alpha$  on the y axis.

2. At  $E > V_0$ , the possible values of the energy are determined by the condition

$$-1 \leq f(E) \leq +1 \quad (2.10)$$

where

$$\begin{aligned} f(E) &= \cos a\alpha \cos b\beta - (\alpha^2 + \beta^2)/2\alpha\beta \sin a\alpha \sin b\beta \\ &= \cos(a\alpha + b\beta) - (\alpha - \beta)^2/2\alpha\beta \sin a\alpha \sin b\beta \end{aligned} \quad (2.11)$$

The energy spectrum will also have a band structure in this case. The relation

$a\alpha + b\beta = n\pi$ ,  $n = 0, 1, 2, \dots$ , which would lead to a discrete spectrum does not satisfy the

inequality of equation 2.8. Substituting  $a\alpha = n(\pi/2) - \varphi$  and  $b\beta = (\pi/2) + \varphi$  into equation

2.11, we find that

$$\begin{aligned} f(E) &= 1 + (\alpha - \beta)^2/2\alpha\beta \sin^2\varphi > 1 \quad \text{for } n \text{ even} \\ &= -1 - (\alpha - \beta)^2/2\alpha\beta \cos^2\varphi < -1 \quad \text{for } n \text{ odd} \end{aligned} \quad (2.11)$$

As the barrier width increases, the miniband width decreases until we simply have discrete levels, as in the case of the quantum well. It is important to know that the  $E$  vs.  $k_x$  relation obtained from the superlattice gives a new effective mass in the superlattice direction.

When the barriers are very thin, this mass is just the starting mass  $m$  used in equation 2.1.

But in the extreme limit of large barriers, the mass becomes infinite.

Even though we have minibands in the one-dimensional superlattice, the real superlattices are 3-D structures. When the transverse energy  $E_{\perp}$  of equation 2.2 is added to the bandstructure, there is no "real energy gap" in the bandstructure. However, if an electron is moving in the  $x$ -direction, and does not suffer any scattering, i.e., does not change its wavevector, it will see a discontinuity in the  $E$  vs.  $k_x$  relation and consequently will be affected as if there was an energy gap present.

The Kronig-Penney model is a very simple description of the superlattice bandstructure.

We will try to use a more refined method, the tight-binding method, to obtain the complete electronic bandstructure of the superlattice. [14]

## **2.5 Practical Example: Negative Differential Conductance in Superlattices**

Since we mentioned how superlattices are expected to improve the electronic characteristics that devices built with bulk semiconductors have, we present some attempts to achieve negative differential conductance in superlattices. Devices built with these superlattices could replace the Gunn amplifiers/oscillators in a new generation of high speed, high frequency devices.



Mollot, Sibille, Palmier, Wang, and Esnault [20] obtained negative differential conductance from a GaAs/AlAs superlattice at 300K. They demonstrated that this negative differential conductance is strongly enhanced at microwave frequencies close to the inverse transit time of the electrons.

Hadjazi, Sibille, Palmier, and Mollot [21] demonstrated that the superlattice negative differential conductance was not due to intervalley transfer like in Gunn devices. They showed that Gunn and superlattice diodes may appear similar, but their different microscopic origin may give to the superlattices several advantages. For instance, electrons in Gunn diodes must initially be heated before transferring into the upper valley so that the electronic temperature may be higher in Gunn than in superlattice devices; hence, superlattice oscillators may inherently be less noisy. Furthermore, their ultimate frequency should only be limited by the intraminiband scattering time, estimated to be of the order of 0.1 ps. In contrast, in transferred electron devices, the velocity is limited by intervalley scattering and takes much longer (1 to 2 ps). These arguments are clearly encouraging for the future of superlattice oscillators or other microwave devices.

## EFFECTS OF LATERAL CONFINEMENT IN A SUPERLATTICE

### III. Two Dimensional Confinement in Semiconductors

There has been some interest in pursuing research in quasi 1-D semiconductor structures because of their exciting potential. This potential is mainly due to the nature of the eigenstates, eigenenergies, and density of states. We hope that our current research will add to the knowledge and interest about these structures.

#### 3.1 Theory

We are interested in studying superlattices that are confined in two dimensions, leaving free only the direction perpendicular to the superlattice. When the confinement in two directions exhibits dimensions smaller than the carrier deBroglie wavelength, the energy levels are quantized and these structures will be defined as quantum well wires. Let's say that our semiconductor has been grown on the  $x$  direction. If the semiconductor is confined in the  $y$  and  $z$  directions (with  $L_y$  and  $L_z$  becoming the new "actual" dimensions of the semiconductor), we will have a wavefunction of the form

$$\psi_k = (L_x)^{-1/2} g_n(z) g_l(y) e^{ik_x x} \quad (3.1)$$

where the envelope functions for an infinite barrier case have the usual form

$$g_n(z) = (2/L_z)^{1/2} \cos(n\pi z/L_z), \text{ for } n \text{ odd} \quad (3.2)$$

$$g_n(z) = (2/L_z)^{1/2} \sin(n\pi z/L_z), \text{ for } n \text{ even}$$

where the well extends from  $z = -L_z/2$  to  $z = +L_z/2$ . Similar eigenfunctions pertain for  $g_l(y)$ . [14]

The electron energies are

$$E_{n,l} = \hbar^2/8\pi^2 m^* [(n\pi/L_z)^2 + (l\pi/L_y)^2] + \hbar^2 k_x^2/8\pi^2 m^* \quad (3.3)$$

This will produce a density of states of the form

$$N(E) = \sum_{n,l} [4\pi(2m)^{1/2}/h] (E - E_{n,l})^{-1/2} \quad (3.4)$$

where  $E_{n,l}$  are the various subband levels. An important effect of this quantization is that once  $L_y$  and  $L_z$  approach 500 Angstroms or less, there is enough inter-subband separation ( $\geq 50$  meV) that there is no inter-subband scattering. The scattering in the same subband is severely restricted for the 1-D system. Overall this results in a severe suppression of scattering and mobilities as high as  $10^7 \text{ cm}^2 \text{ V}^{-1} \text{ s}^{-1}$  have been predicted.

### 3.2 Fabrication of 1-D semiconductor structures

So far, the experimental picture of superior transport in 1-D systems has not been very good. This appears to be linked to the growth and fabrication difficulties. Unlike quantum wells, the fabrication of quantum wires usually involves complex etching/regrowth steps that probably introduce serious defects that affect the transport properties.

In recent years, several schemes for fabricating such structures have been proposed.

These may be divided into two classes. In the first category, a reduction in the system dimensionality is imposed by an external field (magnetic or electrostatic) applied to the free electron gas. In general, this approach requires the use of a quantum well structure if

high magnetic fields are used. [22] Localized lithography with a structure containing a quantum well as well as additional sophisticated processing are required to achieve the additional confinement [23,24] with the use of electrostatic fields. So far the only demonstrations of one and zero degree confinement in GaAs/AlAs structures have been those of Arakawa *et al* [22] who used high magnetic fields on GaAs lasers or quantum wells to demonstrate the effect of 2 and 3 dimensional confinement on laser device characteristics.

The second category of structures attempts to achieve confinement effects using mesa type structures. [25, 26, 27] Because of the extremely small dimensions of the mesa structures, surface depletion layer effects due to deep traps become important and the characteristics of these structures are affected by these defects. Most of the important results using this approach have been obtained on silicon devices. [27] The results on GaAs structures [25] and InP [26] have been unclear and their interpretation remains difficult.

The alternative scheme for increasing the degrees of carrier confinement is to use a locally "built in" crystal potential within the structure. The first attempt used the anisotropic chemical etching of a GaAs quantum well superlattice and the regrowth of wider band gap GaAlAs by MBE. [28] The main difficulty with this approach resided in controlling the accuracy of the anisotropic etching and the quality of the regrown MBE layer. The main problems associated with achieving a uniform etching of the mesa structure and the regrowth of the AlGaAs cladding layer on the etched AlGaAs parts of the mesa structure were not completely solved. A new spectral luminescence feature was observed on

quantum well wires fabricated by this method and attributed to strain effects associated with the structure geometry.

A different approach to building a localized crystal potential that did not involve any lithography was later proposed. With this method, fractional alternate monolayers of GaAlAs and GaAs are deposited by MBE on a vicinal (100) oriented GaAs substrate. [29] The period of the vertical superlattice is controlled by the misorientation angle while the superlattice perfection is function of the degree of ordering. The obtention of such structures requires that growth is taking place in a layer mode and that nucleation is initiated at step edges. [29] The presence of thermally induced kinks at the step edges had initially prevented the obtention of these vertical superlattices. However, there is indication that such structures have been fabricated using atomic layer epitaxy by MOCVD. [30, 31]; the degree of perfection or ordering in these vertical superlattices remains to be evaluated.

The new growth methods that use a "growth interruption" [32] between deposition of each fractional monolayer or the atomic layer epitaxy [33] method should minimize the density of thermal kinks and improve the perfection of such structures.

A new approach in manufacturing 1D and 0D structures relies on intermixing locally the narrow and wider band gap material. Such intermixing produces regions of the material with a band gap intermediate with that of the two original materials. [34, 35] The localized intermixing is achieved in the case of GaAs/AlGaAs quantum wells by interdiffusing selectively the Ga and Al across the interface.

### 3.3 Two Dimensional Confinement in Superlattices

It has been proposed by Weichold [36] that confining superlattices in two dimensions (perpendicular to the direction of growth of the superlattice) can result in modifications to the bandstructure of the superlattice.

The proposed device can be built by growing a superlattice using molecular beam epitaxy (MBE) and etching to produce a mesa array. [37] Figure 3.1 shows this mesa array.



**Figure 3.1** SEM photograph of an etched MBE mesa array [37]

Each mesa must have very small dimensions in the  $y$  and  $z$  directions, and would then be covered by a layer of bulk semiconductor on its sides, leaving the top part of the mesa uncovered. The device will have three terminals: the bulk semiconductor will act as a gate terminal, and the two ends of the superlattice will act as source and gate. When voltage is

applied to the bulk semiconductor, a depletion region around the superlattice will be created by the resulting electric field, further confining the superlattice in the  $y$  and  $z$  directions. The only free dimension will be the  $x$  direction, which is the direction of growth of the superlattice.

It would be interesting to know how the electronic bandstructure of the superlattice changes with varying bulk voltage, and what would the current-voltage characteristics of the device be. We know that when electric charge carriers travel exclusively in one direction in a superlattice, they will only "see" the minibands in that particular direction. Therefore, the electric charge carriers will see gaps in the electronic bandstructure that will make the material have a "different" bandgap and will give the carriers a different effective mass.

In addition, we want to know if the electronic bandstructure in the direction of the current (the  $x$  direction in this case) will be affected. We believe that there will be some band bending, band folding, and/or band splitting.

Our approach is to create computer simulations that will reproduce the known electronic bandstructures of superlattices, and then apply some confining conditions in two dimensions to observe the effects of the two-dimensional confinement. The fabrication of such a structure also creates particular problems that will be analyzed at a later stage of our study.

### 3.4 The tight binding method

In order to study the electronic bandstructure of superlattices, we have chosen the tight binding method, or linear combination of atomic orbitals (LCAO). It is a powerful and flexible empirical technique, and it is capable of providing a reasonably good description of the bandstructure of semiconductors. Explaining the tight binding method is beyond the purpose of this text, and we will limit ourselves to summarize it and to point out the best sources to learn about it.

The method uses a series of approximations and simplifications made to the crystal hamiltonian. The most accurate hamiltonian which can be written for a crystal consists of the kinetic energy of each electron, the kinetic energy of each nucleus, the potential of each electron in the field of each other electron, the potential of each electron in the field of each nucleus, and the potential of each nucleus in the field of each other nucleus. For a macroscopic crystal, this hamiltonian would have a prohibitive number of variables, much too large to even think of solving completely. [38]

The tight binding method comes about from the approximation that the electrons are 'tightly bound' to the atoms within the crystal. Thus, the crystal wave functions should resemble sums of the one atom wave functions of its component atoms. Because of this, the basis states which are used to expand the crystal states are taken to be the one atom states, or the 'orbitals' of the component atoms. The method was proposed by Bloch [39], and much of the currently used formalism is due to Slater and Koster. [40] More information on the tight binding method is also given by Chadi *et al* [41, 42], Chelikowski



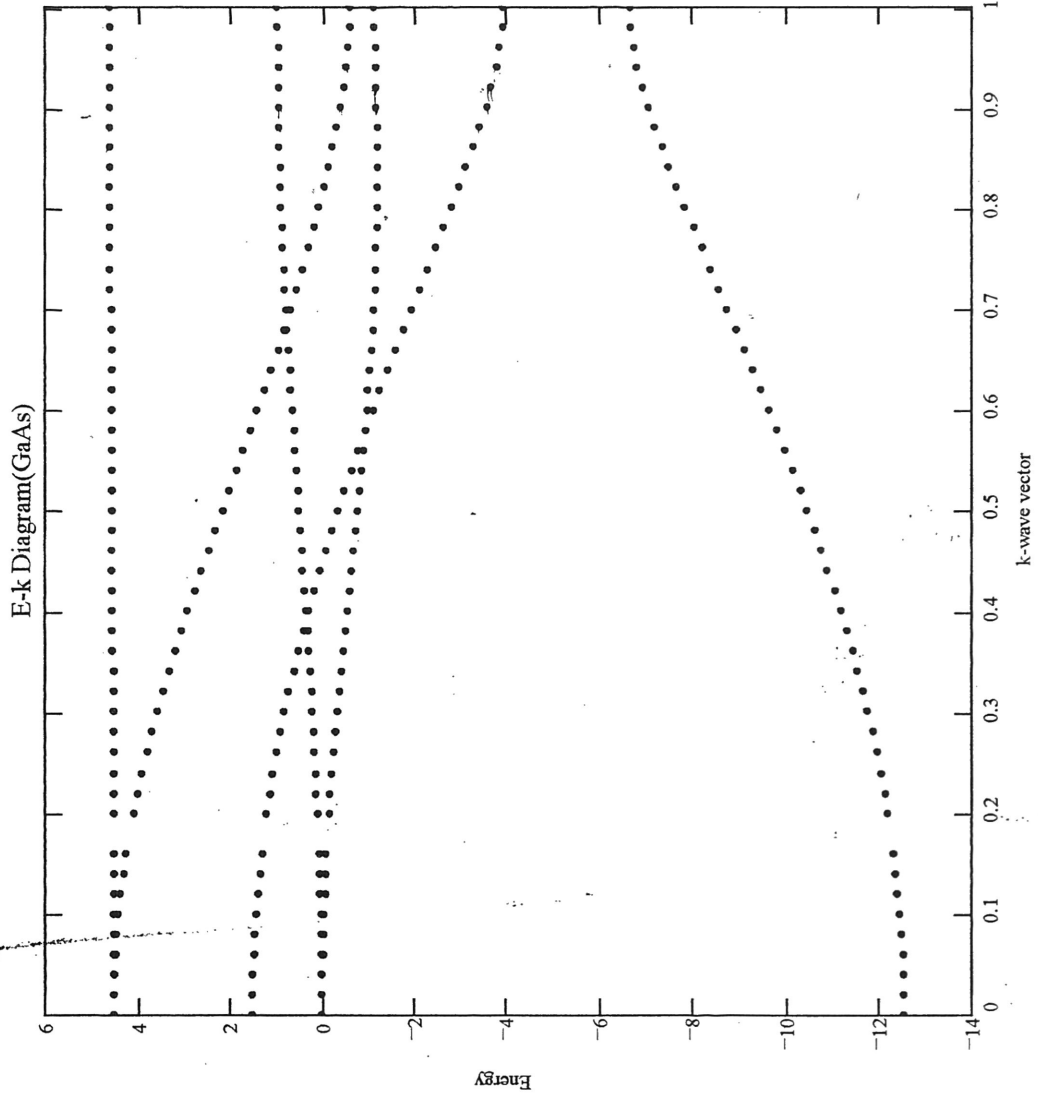
and Cohen [43], and Vogl [44]. Nara [45] has a good article on using the tight binding method for superlattices.

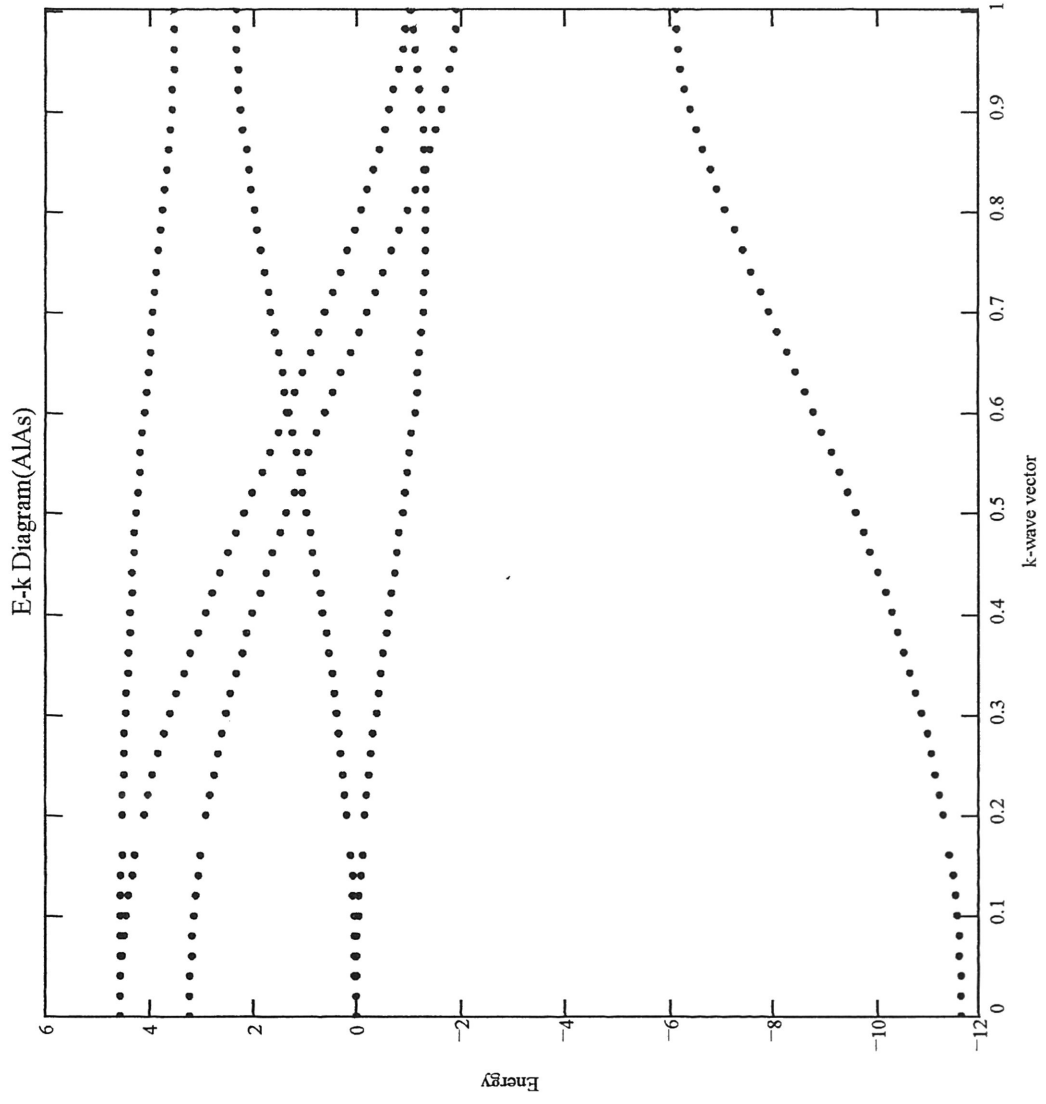
We are currently working on using the tight binding method to obtain the bandstructure of semiconductors. Our results are shown on the next two pages. The bandstructure of GaAs that we obtained is similar to the actual bandstructure of GaAs; however, there are several mistakes. The first and most obvious mistake is that the valence and conduction bands overlap. Also, most of the bands have a correct shape, but not all of them. The bandstructure of AlAs shows similar errors; in fact, it is not very similar to the actual bandstructure of AlAs. The programs used to calculate these bandstructures are shown on Appendix A.

The origins of the errors rely on the equations that describe the interorbital interaction energies in the crystal. We have used equations derived in the past by other researchers, and there is probably some errors in them. We attempt to fix them by re-deriving these equations. In the case of bulk semiconductors, such as GaAs and InAs, we will use only the most nearest neighbors in the lattice to calculate the bandstructure. However, in superlattices, we most attempt to use second and even third nearest neighbors in the lattice to achieve precise results.

The calculation of the bandstructure when the superlattice is confined in two dimensions will be achieved by starting from equations similar to equations 3.1, 3.2, 3.3, and 3.4.

After the confinement conditions have been written, we include them in the tight binding method. These equations will act as “perturbations” of the normal crystal lattice. In the tight binding calculations, they will also look like “perturbations.”





We believe that these “perturbations” will cause the electronic bandstructure of the superlattice to change. Once we have obtained the bandstructure of confined superlattices, we must use it to obtain data such as effective masses and bandgaps. With this information, we can perform Monte Carlo simulations to obtain the resulting I-V characteristic of the laterally confined superlattice.

## REFERENCES

1. Gunn, J.B., "Microwave Oscillations of Current in III-V Semiconductors," *Solid State Communications*, Vol. 1, pp. 88-91, 1963.
2. B.K. Ridley and Watkins, T.B., "The Possibility of Negative Resistance Effects in Semiconductors," *Proc. Phys. Soc.*, Vol. 78, pp. 293-304, 1961.
3. Hilsum, C., "Transferred Electron Amplifiers and Oscillators," *Proceedings of the IRE*, Vol. 50, pp. 185-189, 1962.
4. Kroemer, H., "Negative Conductance in Semiconductors," *IEEE Spectrum*, Vol. 5, pp. 47-56, 1968.
5. David Colliver and Prew, Brian, "Indium Phosphide: is it practical for solid state microwave sources?," *Electronics*, pp. 110-113, 1972.
6. R. Kamoua *et al*, "Development of an Appropriate Model for the Design of D-Band InP Gunn Devices," *Advanced Concepts*, 1993 IEEE/Cornell Conference.
7. P.A. Rolland *et al*, "Comparison Between InP and Other Semiconductor Materials for the Realization of Millimeter Wave Two Terminal Devices," Indium Phosphide and Related Materials International Conference, 1990.
8. Ludwig, Gerald, "Gunn Effect in CdTe," *IEEE Transactions of Electron Devices*, Vol. ED-14, No. 9, pp. 547-552, 1967.
9. Y. Takeda, N. Shikagawa, and Sasaki, A., "Transferred-Electron Oscillation in  $n$ -In<sub>0.53</sub>Ga<sub>0.47</sub>As," *Solid State Electronics*, Vol. 23, pp. 1003-1006, 1979.
10. W. Kowalsky and Schlachetzki, A., "InGaAs Gunn Oscillators," *Electronic Letters*, Vol. 20, No. 12, pp. 502-503, 1984.
11. Allen, J.W. *et al*, "Microwave Oscillations in GaAs<sub>x</sub>P<sub>1-x</sub> Alloys," *Applied Physics Letters*, Vol. 7, No. 4, pp. 78-80, 1965.
12. L. Esaki and Tsu, R., "Superlattice and Negative Differential Conductivity in Semiconductors," *IBM Journal of Research and Development*, January 1970, pp. 61-65.
13. Capasso, F., "Band Structure Engineering and its Device Applications," *Semiconductor Superlattices and Interfaces*, pp. 379, 1993.
14. Singh, Jasprit, Physics of Semiconductors and their Heterostructures, pp. 49, McGraw-Hill, 1993

15. M.B. Panish and Sumski, S., *Journal of Applied Physics*, vol. 55, pp. 3571-3576, May 1984.
16. M. Razeghi and Duchemin, J.P., "Recent advances in MOCVD growth of  $\text{In}_x\text{Ga}_{1-x}\text{As}_y\text{P}_{1-y}$  alloys," *J. Crystal Growth*, vol. 70, pp. 145-149, 1984.
17. Tsang, W.T., "Chemical beam epitaxy of InP and GaAs," *Applied Physics Letters*, vol. 45, pp. 1234-1236, Dec. 1984.
18. H. Fujiyasu, H. Takahashi, H. Shimizu, and Sasaki, A., "Optical properties of ZnS-ZnSe superlattices prepared by a HWE," in *Proc. 17th International Conf. Phys. Semiconductors*, San Francisco, CA, Aug. 1984, pp. 539-542.
19. M. Pessa and Jylha, O., "Growth of  $\text{Cd}_{1-x}\text{Mn}_x\text{Te}$  films with  $0 < x < 0.9$  by atomic layer epitaxy," *Appl. Phys. Letters*, vol. 45, pp. 646-648, Sept., 1984.
20. Sibille, Palmier, Wang, Esnault, and Mollot, "DC and microwave negative differential conductance in GaAs/AlAs superlattices," *Applied Physics Letters*, vol. 56, p. 256-258, 1990.
21. Hadjazi, Sibille, Palmier, Mollot, "Negative Differential Conductance in GaAs/AlAs Superlattices," *Electronic Letters*, vol. 27, No. 12, pp. 1101-1103, 1991.
22. Y. Arakawa, K. Vahala, A. Yariv, K. Lau, *Appl. Phys. Lett.*, vol. 47, pp. 142, 1985.
23. H. Sasaki, *Jpn. J. Appl. Phys.*, vol. 19, pp. L735, 1980.
24. S. Luryi, F. Capasso, *Appl. Phys. Lett.*, vol. 47, pp. 1348, 1985.
25. M.A. Reed, R.T. Bate, K. Bradshaw, W.M. Duncan, W.R. Frensley, J.W. Lee, H.D. Shi, *Journal Vac. Sci. Technol.*, vol. B4(1), pp. 358, 1986.
26. H. Temkins, G.J. Dolan, M.B. Panish, S.W.G. Chen, *Appl. Phys. Letters*, vol. 50, pp. 415, 1987.
27. W.J. Skocpol, L.D. Jackel, E.L. Hei, R.E. Howard, C.A. Fetter, *Phys. Rev. Lett.*, vol. 49, pp. 951, 1981.
28. P.M. Petroff, A.C. Gossard, R.A. Logan, W. Wiegmann, *Appl. Phys. Lett.*, vol. 41, pp. 635, 1982.
29. P.M. Petroff, A.C. Gossard, W. Wiegmann, *Appl. Phys. Lett.*, vol. 45, pp. 620, 1984.
30. S. Yamada, T. Fukui, H. Saito, *J. Vac. Sci. Tech*, vol. 50, pp. 329, 1987.

31. T. Fukui, H. Saito, *J. Vac. Sci. Tech*, vol. 50, pp. 824, 1987.
32. C. W. Tu, R.C. Miller, B.A. Wilson, P.M. Petroff, T.D Harris, R.F. Kopf, S.K. Spitz, M.G. Lamont, *J. Crystal Growth*, vol. 81, pp. 159, 1987.
33. T. Fuki, H. Saito, *Jpn. J. Appl. Phys.*, vol. 23, pp. L521, 1984.
34. J. Cibert, P.M. Petroff, D.J. Werder, S.J. Pearton, A.C. Gossard, J.H. English, *Appl. Phys. Lett.*, vol. 49, pp. 223, 1986.
35. Y. Hirayama, Y. Suzuki, H. Okamoto, *Jpn. Appl. Phys.*, vol. 24, pp. 1498, 1985.
36. M.H. Weichold, oral communication to the author
37. W.B. Kinard, M.H. Weichold, W.P. Kirk, "Fabrication of a gated gallium arsenide heterostructure resonant tunneling diode," *J. Vac. Sci. Technol.*, vol. B 8(3), pp. 393-396, May/June 1990.
38. M. Jaffe, Ph.D. thesis, Univ. of Michigan, 1989.
39. F. Bloch, "Quantum mechanics of electrons in crystal lattices," *Zeitschrift fur Physik*, 52(7-8), pp. 555, 1928.
40. J. Slater, F. Koster, "Simplified LCAO method for the periodic potential problem," *Physical Review* 94(6), p. 1498, 1954.
41. D.J. Chadi, M.L. Cohen, "Tight Binding Calculations of the Valence Bands of Diamond and Zincblende Crystals", *Phys. Stat. Sol.(B)*, vol. 68, pp. 405, 1975.
42. D.J. Chadi, "Spin-orbit splitting in crystalline and compositionally disordered semiconductors," *Physical Review B*, vol. 16, no.2, pp. 790, 1977.
43. J.R. Chelikowski, M.L. Cohen, "Nonlocal pseudopotential calculations for the electronic structure of eleven diamond and zinc-blende semiconductors," *Physical Review B*, vol. 14, no. 2, pp. 556, 1976.
44. P. Vogl, "A semi-empirical tight-binding theory of the electronic structure of semiconductors," *J. Phys. Chem. Solids*, vol. 4, no.5, pp. 365-378, 1983.
45. S. Nara, "An improved tight binding band structure calculation, of  $(\text{GaAs})_n/(\text{AlAs})_n$  ( $n=1-4$ ) superlattices", *Japanese Journal of Applied Physics*, vol. 26(5), p. 690, 1987.

APPENDIX A  
MATHLAB PROGRAM



```

% Program to produce the electronic bandstructure of GaAs
% Julio Toro da Silva
% Member of the Research Group of Dr. Mark H. Weichold
% Department of Electrical Engineering
% Texas A&M University
% College Station, Texas
% February 1996

```

```

a = 5.65E-10; % lattice constant of GaAs

```

```

% Interaction energies in GaAs, in eV, from Talwar and Ting, 1982

```

```

p1 = -6.72357; % Ess(000)0 in eV for GaAs
p2 = -3.97833; % Ess(000)1 in eV for GaAs
p3 = 0.64095; % Exx(000)0
p4 = 2.87407; % Exx(000)1
p5 = -6.90000; % 4Ess(0.5,0.5,0.5)
p6 = 5.24000; % 4Esx(0.5,0.5,0.5)01
p7 = 4.32100; %
p8 = 2.00000;
p9 = 5.50000;
p10 = -0.33905;
p11 = -1.75633;
p12 = 0.60000;
p13 = 0.96000;
p14 = 0.44445;
p15 = 1.12077;
p16 = 0.04520;
p17 = 0.09640;
p18 = -0.04738;
p19 = -0.06533;
p20 = 0.78000;
p21 = -0.08000;
p22 = 0;
p23 = 0;

```

```

pi = 3.14159;

```

```

for x=1:100

```

```

    kx(x)=x/100;
    ky=0;
    kz=0;
    c1 = cos (pi*kx(x));
    c2 = cos (pi*ky);
    c3 = cos (pi*kz);
    s1 = sin (pi*kx(x));
    s2 = sin (pi*ky);
    s3 = sin (pi*kz);
    g0 = cos(pi*kx(x)/2)*cos(pi*ky/2)*cos(pi*kz/2) - i*sin(pi*kx(x)/2)*sin(p
    g1 = -cos(pi*kx(x)/2)*sin(pi*ky/2)*sin(pi*kz/2) + i*sin(pi*kx(x)/2)*cos(
    g2 = -sin(pi*kx(x)/2)*cos(pi*ky/2)*sin(pi*kz/2) + i*cos(pi*kx(x)/2)*sin(
    g3 = -sin(pi*kx(x)/2)*sin(pi*ky/2)*cos(pi*kz/2) + i*cos(pi*kx(x)/2)*cos(

    matr(1,1) = p1 + p18*(c1*c2 + c2*c3 + c3*c1);
    matr(1,5) = p5*g0;
    matr(5,1) = matr(1,5);
    matr(5,5) = p2 + p19*(c1*c2 + c2*c3 + c3*c1);
    matr(1,2) = -p20*s2*s3 + i*p16*s1*(c2+c3);
    matr(2,1) = matr(1,2);
    matr(5,2) = -p7*conj(g1);

```

```

matr(2,5) = matr(5,2);
matr(2,2) = p3 + p14*c1*(c2+c3) + p10*c2*c3;
matr(1,3) = -p20*s1*s3 + i*p16*s2*(c3+c1);
matr(3,1) = matr(1,3);
matr(5,3) = -p7*conj(g2);
matr(3,5) = matr(5,3);
matr(2,3) = -p12*s1*s2 - i*p22*c3*(s1-s3);
matr(3,2) = matr(2,3);
matr(3,3) = p3 + p14*c2*(c1+c3) + p10*c1*c3;
matr(1,4) = -p20*s1*s3 + i*p16*s3*(c1+c2);
matr(4,1) = matr(1,4);
matr(5,4) = -p7*g3;
matr(4,5) = matr(5,4);
matr(2,4) = -p12*s1*s3 - i*p22*c2*(s1-s3);
matr(4,2) = matr(2,4);
matr(3,4) = -p12*s2*s3 - i*p22*c1*(s2-s3);
matr(4,3) = matr(3,4);
matr(4,4) = p3 + p14*c3*(c1+c2) + p10*c1*c2;
matr(1,6) = p6*g1;
matr(6,1) = matr(1,6);
matr(5,6) = p21*s1*s2 + i*p17*s1*(c2+c3);
matr(6,5) = matr(5,6);
matr(2,6) = p8*g0;
matr(6,2) = matr(2,6);
matr(3,6) = p9*g3;
matr(6,3) = matr(3,6);
matr(4,6) = p9*g2;
matr(6,4) = matr(4,6);
matr(6,6) = p4 + p15*c1*(c2+c3) + p11*c2*c3;
matr(1,7) = p6*g2;
matr(7,1) = matr(1,7);
matr(5,7) = p21*s1*s3 + i*p17*s2*(c1+c3);
matr(7,5) = matr(5,7);
matr(2,7) = p9*g3;
matr(7,2) = matr(2,7);
matr(3,7) = p8*g0;
matr(7,3) = matr(3,7);
matr(4,7) = p9*g1;
matr(7,4) = matr(4,7);
matr(6,7) = -p13*s1*s2 + i*p23*c3*(s1-s2);
matr(7,6) = matr(6,7);
matr(7,7) = p4 + p15*c2*(c3+c1) + p11*c1*c3;
matr(1,8) = p6*g3;
matr(8,1) = matr(1,8);
matr(5,8) = p23*s1*s2 + i*p1*s3*(c1+c2);
matr(8,5) = matr(5,8);
matr(2,8) = p9*g2;
matr(8,2) = matr(2,8);
matr(3,8) = p9*g1;
matr(8,3) = matr(3,8);
matr(4,8) = p6*g0;
matr(8,4) = matr(4,8);
matr(6,8) = -p13*s1*s3 + i*p23*c2*(s1-s3);
matr(8,6) = matr(6,8);
matr(7,8) = -p13*s2*s3 + i*p23*c1*(s2-s3);
matr(8,7) = matr(7,8);
matr(8,8) = p4 + p15*c3*(c1+c2) + p11*c1*c2;

```

```

% Solve for eigenvalues
lambda = eig(matr);

```

```
mout(1:8,x) = lambda;
```

```
end
```

```
plot (kx,mout);  
title ('E vs. k, for GaAs, from 000 to 100');  
xlabel('k');  
ylabel('E');
```

APPENDIX B  
MATHCAD PROGRAM

```

.MCAD 304020000 1 79 3472 0
.CMD PLOTFORMAT
0 0 1 1 1 0 0 1 1
0 0 1 1 1 0 0 1 1
1 0 6 0 7 7 NO-TRACE-STRING
0 2 1 0 1 1 NO-TRACE-STRING
0 3 2 0 1 1 NO-TRACE-STRING
0 4 3 0 1 1 NO-TRACE-STRING
0 1 4 0 1 1 NO-TRACE-STRING
0 2 5 0 1 1 NO-TRACE-STRING
0 3 6 0 1 1 NO-TRACE-STRING
0 4 0 0 1 1 NO-TRACE-STRING
0 1 1 0 1 1 NO-TRACE-STRING
0 2 2 0 1 1 NO-TRACE-STRING
0 3 3 0 1 1 NO-TRACE-STRING
0 4 4 0 1 1 NO-TRACE-STRING
0 1 5 0 1 1 NO-TRACE-STRING
0 2 6 0 1 1 NO-TRACE-STRING
0 3 0 0 1 1 NO-TRACE-STRING
0 4 1 0 1 1 NO-TRACE-STRING
0 1 1 21 15 0 0 3
.CMD FORMAT rd=d ct=10 im=i et=3 zt=15 pr=3 mass length time charge temperature t
.CMD SET ORIGIN 0
.CMD SET TOL 0.0010000000000000
.CMD SET PRNCOLWIDTH 8
.CMD SET PRNPRECISION 4
.CMD PRINT_SETUP 1.000000 1.000000 1.000000 1.000000 0
.CMD HEADER_FOOTER 1 1 *empty* *empty* *empty* 0 1 *empty* *empty* *empty*
.CMD HEADER_FOOTER_FONT fontID=14 family=Arial points=10 bold=0 italic=0 underline
.CMD HEADER_FOOTER_FONT fontID=15 family=Arial points=10 bold=0 italic=0 underline
.CMD DEFAULT_TEXT_PARPROPS 0 0 0
.CMD DEFINE_FONTSTYLE_NAME fontID=0 name=Variables
.CMD DEFINE_FONTSTYLE_NAME fontID=1 name=Constants
.CMD DEFINE_FONTSTYLE_NAME fontID=2 name=Text
.CMD DEFINE_FONTSTYLE_NAME fontID=4 name=User^1
.CMD DEFINE_FONTSTYLE_NAME fontID=5 name=User^2
.CMD DEFINE_FONTSTYLE_NAME fontID=6 name=User^3
.CMD DEFINE_FONTSTYLE_NAME fontID=7 name=User^4
.CMD DEFINE_FONTSTYLE_NAME fontID=8 name=User^5
.CMD DEFINE_FONTSTYLE_NAME fontID=9 name=User^6
.CMD DEFINE_FONTSTYLE_NAME fontID=10 name=User^7
.CMD DEFINE_FONTSTYLE fontID=0 family=Times^New^Roman points=10 bold=0 italic=0 un
.CMD DEFINE_FONTSTYLE fontID=1 family=Times^New^Roman points=10 bold=0 italic=0 un
.CMD DEFINE_FONTSTYLE fontID=2 family=Arial points=10 bold=1 italic=0 underline=1
.CMD DEFINE_FONTSTYLE fontID=4 family=Arial points=10 bold=0 italic=0 underline=0
.CMD DEFINE_FONTSTYLE fontID=5 family=Courier^New points=10 bold=0 italic=0 underl
.CMD DEFINE_FONTSTYLE fontID=6 family=System points=10 bold=0 italic=0 underline=0
.CMD DEFINE_FONTSTYLE fontID=7 family=Script points=10 bold=0 italic=0 underline=0
.CMD DEFINE_FONTSTYLE fontID=8 family=Roman points=10 bold=0 italic=0 underline=0
.CMD DEFINE_FONTSTYLE fontID=9 family=Modern points=10 bold=0 italic=0 underline=0
.CMD DEFINE_FONTSTYLE fontID=10 family=Times^New^Roman points=10 bold=0 italic=0 u
.CMD UNITS U=1
.CMD DIMENSIONS_ANALYSIS 0 0
.CMD COLORTAB_ENTRY 0 0 0
.CMD COLORTAB_ENTRY 128 0 0
.CMD COLORTAB_ENTRY 0 128 0
.CMD COLORTAB_ENTRY 128 128 0
.CMD COLORTAB_ENTRY 0 0 128
.CMD COLORTAB_ENTRY 128 0 128
.CMD COLORTAB_ENTRY 0 128 128

```



```

{0:kx}NAME)/(2))*{0:sin}NAME({0:\p}NAME*({0:ky}NAME)/(2))*{0:sin}NAME({0:\p}NAME*
{0:Im}NAME({0:sin}NAME({0:\p}NAME*({0:kx}NAME)/(2))*{0:cos}NAME({0:\p}NAME*({0:ky}
({0:\p}NAME*({0:kz}NAME)/(2))+{0:Im}NAME({0:cos}NAME({0:\p}NAME*({0:kx}NAME)/(2))*
*({0:ky}NAME)/(2))*{0:cos}NAME({0:\p}NAME*({0:kz}NAME)/(2))+{0:Im}NAME({0:cos}NAME
{0:C1}NAME*({0:C2}NAME+{0:C3}NAME)+{0:P11}NAME*{0:C2}NAME*{0:C3}NAME))){71}AME){72
{0:P21}NAME*{0:S1}NAME*{0:S2}NAME+{0:Im}NAME({0:P17}NAME*{0:S1}NAME*({0:C2}NAME+{0
{0:C2}NAME))){71}AME){72}3}NAME+{0:P14}NAME*{0:C3}NAME*({0:C1}NAME+{0:C2}NAME)+{0:
))){71}AME){72}12}NAME*{0:S2}NAME*{0:S3}NAME-{0:Im}NAME((({0:P12}NAME*{0:C1}NAME*
){71}AME){72}12}NAME*{0:S1}NAME*{0:S3}NAME-{0:Im}NAME({0:P12}NAME*{0:C2}NAME*({0:S
(-{0:P7}NAME*{0:g3}NAME))){71}AME){72}20}NAME*{0:S1}NAME*{0:S3}NAME+{0:P16}NAME*{0
{0:Im}NAME({0:P17}NAME*{0:S3}NAME*({0:C1}NAME+{0:C2}NAME))){71}AME){72}3}NAME+{0
){72}12}NAME*{0:S1}NAME*{0:S2}NAME-{0:Im}NAME({0:P22}NAME*{0:C3}NAME*({0:S1}NAME-
{0:P11}NAME*{0:C1}NAME*{0:C3}NAME))){71}AME){72}13}NAME*{0:S1}NAME*{0:S2}NAME+{0:I
*({0:C3}NAME+{0:C1}NAME))){71}AME){72}3}NAME+{0:P14}NAME*{0:C1}NAME*({0:C2}NAME+
))){71}AME){72}8}NAME*{0:g0}NAME))){71}AME){72}20}NAME*{0:S2}NAME*{0:S3}NAME+{0:I
{72}2}NAME+{0:P19}NAME*({0:C1}NAME*{0:C2}NAME+{0:C2}NAME*{0:C3}NAME+{0:C3}NAME*{0:
{0:P5}NAME*{0:g0}NAME))){71}AME){72}1}NAME+{0:P18}NAME*({0:C1}NAME*{0:C2}NAME+{0:C
{0:px1pz1}NAMEö{0:s1pz1}NAMEö{0:pz0pz1}NAMEö{0:py0pz1}NAMEö{0:px0pz1}NAMEö{0:s0pz1
{0:s1px1}NAMEö{0:pz0px1}NAMEö{0:py0px1}NAMEö{0:px0px1}NAMEö{0:s0px1}NAMEö{0:s1pz1}
{0:pz0pz0}NAMEö{0:py0pz0}NAMEö{0:px0pz0}NAMEö{0:s0pz0}NAMEö{0:py0pz1}NAMEö{0:py0py
{0:px0py0}NAMEö{0:px0px0}NAMEö{0:s0px0}NAMEö{0:s0pz1}NAMEö{0:s0py1}NAMEö{0:s0px1}N
.EQN 192 4 3328 0 0
{0:j}NAME:1;50
.EQN 0 9 3335 0 0
{0:ky}NAME:0
.EQN 0 6 3336 0 0
{0:kz}NAME:0
.EQN 6 -15 3325 0 0
({0:kx}NAME)[({0:j}NAME):0,0.02,0.04,0.06,0.08,0.1,0.12,0.14,0.16,0.2,0.22,0.24,0.
0.98,1
.EQN 3 7 3339 0 0
({0:k}NAME)[({0:j}NAME):((((({0:kx}NAME)[({0:j}NAME)))^(2)+({0:ky}NAME)^(2)+({0:kz
.EQN 10 10 3356 0 0
{0:i}NAME:0;7
.EQN 4 -12 3343 0 0
({0:k}NAME)[({0:j}NAME)=_n_u_l_l_
.EQN 6 9 3465 0 0
{0:E}NAME({0:j}NAME):{0:eigenvals}NAME({0:X}NAME((({0:kx}NAME)[({0:j}NAME)))
.EQN 5 0 3466 0 0
({0:M}NAME)[({0:i}NAME,{0:j}NAME):({0:E}NAME({0:j}NAME))][({0:i}NAME)
.TXT 118 -18 3470 0 0
C x1,1,0,0
.EQN 5 1 3472 0 0
_n_u_l_l_&_n_u_l_l_&(_n_u_l_l_&_n_u_l_l_)&({0:M}NAME)[({0:i}NAME,{0:j}NAME)@1&0&(_
0 0 1 1 1 0 0 1 1 k-wave vector
0 0 1 1 1 0 0 1 1 Energy
0 0 6 0 2 2 NO-TRACE-STRING
0 2 1 0 1 1 NO-TRACE-STRING
0 3 2 0 1 1 NO-TRACE-STRING
0 4 3 0 1 1 NO-TRACE-STRING
0 1 4 0 1 1 NO-TRACE-STRING
0 2 5 0 1 1 NO-TRACE-STRING
0 3 6 0 1 1 NO-TRACE-STRING
0 4 0 0 1 1 NO-TRACE-STRING
0 1 1 0 1 1 NO-TRACE-STRING
0 2 2 0 1 1 NO-TRACE-STRING
0 3 3 0 1 1 NO-TRACE-STRING
0 4 4 0 1 1 NO-TRACE-STRING
0 1 5 0 1 1 NO-TRACE-STRING
0 2 6 0 1 1 NO-TRACE-STRING

```

0 3 0 0 1 1 NO-TRACE-STRING  
0 4 1 0 1 1 NO-TRACE-STRING  
1 1 1 64 58 10 0 3 E-k Diagram(GaAs)



```
.MCAD 304020000 1 79 3472 0
.CMD PLOTFORMAT
0 0 1 1 1 0 0 1 1
0 0 1 1 1 0 0 1 1
1 0 6 0 7 7 NO-TRACE-STRING
0 2 1 0 1 1 NO-TRACE-STRING
0 3 2 0 1 1 NO-TRACE-STRING
0 4 3 0 1 1 NO-TRACE-STRING
0 1 4 0 1 1 NO-TRACE-STRING
0 2 5 0 1 1 NO-TRACE-STRING
0 3 6 0 1 1 NO-TRACE-STRING
0 4 0 0 1 1 NO-TRACE-STRING
0 1 1 0 1 1 NO-TRACE-STRING
0 2 2 0 1 1 NO-TRACE-STRING
0 3 3 0 1 1 NO-TRACE-STRING
0 4 4 0 1 1 NO-TRACE-STRING
0 1 5 0 1 1 NO-TRACE-STRING
0 2 6 0 1 1 NO-TRACE-STRING
0 3 0 0 1 1 NO-TRACE-STRING
0 4 1 0 1 1 NO-TRACE-STRING
0 1 1 21 15 0 0 3
.CMD FORMAT rd=d ct=10 im=i et=3 zt=15 pr=3 mass length time charge temperature t
.CMD SET ORIGIN 0
.CMD SET TOL 0.0010000000000000
.CMD SET PRNCOLWIDTH 8
.CMD SET PRNPRECISION 4
.CMD PRINT_SETUP 1.000000 1.000000 1.000000 1.000000 0
.CMD HEADER_FOOTER 1 1 *empty* *empty* *empty* 0 1 *empty* *empty* *empty*
.CMD HEADER_FOOTER_FONT fontID=14 family=Arial points=10 bold=0 italic=0 underline
.CMD HEADER_FOOTER_FONT fontID=15 family=Arial points=10 bold=0 italic=0 underline
.CMD DEFAULT_TEXT_PARPROPS 0 0 0
.CMD DEFINE_FONTSTYLE_NAME fontID=0 name=Variables
.CMD DEFINE_FONTSTYLE_NAME fontID=1 name=Constants
.CMD DEFINE_FONTSTYLE_NAME fontID=2 name=Text
.CMD DEFINE_FONTSTYLE_NAME fontID=4 name=User^1
.CMD DEFINE_FONTSTYLE_NAME fontID=5 name=User^2
.CMD DEFINE_FONTSTYLE_NAME fontID=6 name=User^3
.CMD DEFINE_FONTSTYLE_NAME fontID=7 name=User^4
.CMD DEFINE_FONTSTYLE_NAME fontID=8 name=User^5
.CMD DEFINE_FONTSTYLE_NAME fontID=9 name=User^6
.CMD DEFINE_FONTSTYLE_NAME fontID=10 name=User^7
.CMD DEFINE_FONTSTYLE fontID=0 family=Times^New^Roman points=10 bold=0 italic=0 un
.CMD DEFINE_FONTSTYLE fontID=1 family=Times^New^Roman points=10 bold=0 italic=0 un
.CMD DEFINE_FONTSTYLE fontID=2 family=Arial points=10 bold=1 italic=0 underline=1
.CMD DEFINE_FONTSTYLE fontID=4 family=Arial points=10 bold=0 italic=0 underline=0
.CMD DEFINE_FONTSTYLE fontID=5 family=Courier^New points=10 bold=0 italic=0 underl
.CMD DEFINE_FONTSTYLE fontID=6 family=System points=10 bold=0 italic=0 underline=0
.CMD DEFINE_FONTSTYLE fontID=7 family=Script points=10 bold=0 italic=0 underline=0
.CMD DEFINE_FONTSTYLE fontID=8 family=Roman points=10 bold=0 italic=0 underline=0
.CMD DEFINE_FONTSTYLE fontID=9 family=Modern points=10 bold=0 italic=0 underline=0
.CMD DEFINE_FONTSTYLE fontID=10 family=Times^New^Roman points=10 bold=0 italic=0 u
.CMD UNITS U=1
.CMD DIMENSIONS_ANALYSIS 0 0
.CMD COLORTAB_ENTRY 0 0 0
.CMD COLORTAB_ENTRY 128 0 0
.CMD COLORTAB_ENTRY 0 128 0
.CMD COLORTAB_ENTRY 128 128 0
.CMD COLORTAB_ENTRY 0 0 128
.CMD COLORTAB_ENTRY 128 0 128
.CMD COLORTAB_ENTRY 0 128 128
```



```

{0:kx}NAME)/(2))*{0:sin}NAME({0:\p}NAME*({0:ky}NAME)/(2))*{0:sin}NAME({0:\p}NAME*
{0:Im}NAME({0:sin}NAME({0:\p}NAME*({0:kx}NAME)/(2))*{0:cos}NAME({0:\p}NAME*({0:ky}
({0:\p}NAME*({0:kz}NAME)/(2))+{0:Im}NAME({0:cos}NAME({0:\p}NAME*({0:kx}NAME)/(2))*
*({0:ky}NAME)/(2))*{0:cos}NAME({0:\p}NAME*({0:kz}NAME)/(2))+{0:Im}NAME({0:cos}NAME
{0:C1}NAME*({0:C2}NAME+{0:C3}NAME)+{0:P11}NAME*{0:C2}NAME*{0:C3}NAME))){71}AME){72
{0:P21}NAME*{0:S1}NAME*{0:S2}NAME+{0:Im}NAME({0:P17}NAME*{0:S1}NAME*({0:C2}NAME+{0
{0:C2}NAME))){71}AME){72}3}NAME+{0:P14}NAME*{0:C3}NAME*({0:C1}NAME+{0:C2}NAME)+{0:
))){71}AME){72}12}NAME*{0:S2}NAME*{0:S3}NAME-{0:Im}NAME((({0:P12}NAME*{0:C1}NAME*
){71}AME){72}12}NAME*{0:S1}NAME*{0:S3}NAME-{0:Im}NAME({0:P12}NAME*{0:C2}NAME*({0:S
(-{0:P7}NAME*{0:g3}NAME))){71}AME){72}20}NAME*{0:S1}NAME*{0:S3}NAME+{0:P16}NAME*{0
{0:Im}NAME({0:P17}NAME*{0:S3}NAME*({0:C1}NAME+{0:C2}NAME))){71}AME){72}3}NAME+{0
){72}12}NAME*{0:S1}NAME*{0:S2}NAME-{0:Im}NAME({0:P22}NAME*{0:C3}NAME*({0:S1}NAME-
{0:P11}NAME*{0:C1}NAME*{0:C3}NAME))){71}AME){72}13}NAME*{0:S1}NAME*{0:S2}NAME+{0:I
*({0:C3}NAME+{0:C1}NAME))){71}AME){72}3}NAME+{0:P14}NAME*{0:C1}NAME*({0:C2}NAME+
]))){71}AME){72}8}NAME*{0:g0}NAME))){71}AME){72}20}NAME*{0:S2}NAME*{0:S3}NAME+{0:I
{72}2}NAME+{0:P19}NAME*({0:C1}NAME*{0:C2}NAME+{0:C2}NAME*{0:C3}NAME+{0:C3}NAME*{0:
{0:P5}NAME*{0:g0}NAME))){71}AME){72}1}NAME+{0:P18}NAME*({0:C1}NAME*{0:C2}NAME+{0:C
{0:px1pz1}NAMEö{0:s1pz1}NAMEö{0:pz0pz1}NAMEö{0:py0pz1}NAMEö{0:px0pz1}NAMEö{0:s0pz1
{0:s1px1}NAMEö{0:pz0px1}NAMEö{0:py0px1}NAMEö{0:px0px1}NAMEö{0:s0px1}NAMEö{0:s1pz1}
{0:pz0pz0}NAMEö{0:py0pz0}NAMEö{0:px0pz0}NAMEö{0:s0pz0}NAMEö{0:py0pz1}NAMEö{0:py0py
{0:px0py0}NAMEö{0:px0px0}NAMEö{0:s0px0}NAMEö{0:s0pz1}NAMEö{0:s0py1}NAMEö{0:s0px1}N
.EQN 192 4 3328 0 0
{0:j}NAME:1;50
.EQN 0 9 3335 0 0
{0:ky}NAME:0
.EQN 0 6 3336 0 0
{0:kz}NAME:0
.EQN 6 -15 3325 0 0
({0:kx}NAME)[({0:j}NAME):0,0.02,0.04,0.06,0.08,0.1,0.12,0.14,0.16,0.2,0.22,0.24,0.
0.98,1
.EQN 3 7 3339 0 0
({0:k}NAME)[({0:j}NAME):((((({0:kx}NAME)[({0:j}NAME)))^(2)+({0:ky}NAME)^(2)+({0:kz}
.EQN 10 10 3356 0 0
{0:i}NAME:0;7
.EQN 4 -12 3343 0 0
({0:k}NAME)[({0:j}NAME)=_n_u_l_l_
.EQN 6 9 3465 0 0
{0:E}NAME({0:j}NAME):{0:eigenvals}NAME({0:X}NAME({0:kx}NAME)[({0:j}NAME)])
.EQN 5 0 3466 0 0
({0:M}NAME)[({0:i}NAME,{0:j}NAME):({0:E}NAME({0:j}NAME))[({0:i}NAME)
.TXT 118 -18 3470 0 0
C x1,1,0,0
.EQN 5 1 3472 0 0
_n_u_l_l_&n_u_l_l_&(n_u_l_l_&n_u_l_l_)&({0:M}NAME)[({0:i}NAME,{0:j}NAME)@1&0&(_
0 0 1 1 1 0 0 1 1 k-wave vector
0 0 1 1 1 0 0 1 1 Energy
0 0 6 0 2 2 NO-TRACE-STRING
0 2 1 0 1 1 NO-TRACE-STRING
0 3 2 0 1 1 NO-TRACE-STRING
0 4 3 0 1 1 NO-TRACE-STRING
0 1 4 0 1 1 NO-TRACE-STRING
0 2 5 0 1 1 NO-TRACE-STRING
0 3 6 0 1 1 NO-TRACE-STRING
0 4 0 0 1 1 NO-TRACE-STRING
0 1 1 0 1 1 NO-TRACE-STRING
0 2 2 0 1 1 NO-TRACE-STRING
0 3 3 0 1 1 NO-TRACE-STRING
0 4 4 0 1 1 NO-TRACE-STRING
0 1 5 0 1 1 NO-TRACE-STRING
0 2 6 0 1 1 NO-TRACE-STRING

```

0 3 0 0 1 1 NO-TRACE-STRING  
0 4 1 0 1 1 NO-TRACE-STRING  
1 1 1 64 58 10 0 3 E-k Diagram(AlAs)